Advanced Journal of Chemistry-Section A

Journal homepage: www.ajchem-a.com

Original Research Article

Electrochemically Synthesize SrSe/ZrSe Heterostructure Material for Photovoltaic Application

Alexander Ighemuno Agbrara [1] *, Ernest Ogheneruona Ojegu [1], Mike Onyekachukwu Osiele [1], Imosobomeh Lucky Ikhioya [2,3]

[1] *Department of Physics, Delta State University, Abraka, Delta State, Nigeria*
[2] *Department of Physics and Astronomy, University of Nigeria, Nsukka, Nigeria*
[3] *National Centre for Physics, Quaid-i-Azam University Campus, Islamabad, Pakistan*

A R T I C L E   I N F O

A B S T R A C T

In this research, SrSe/ZrSe super-lattice was synthesized using an electrochemical deposition technique. The XRD pattern reveals a polycrystalline cubic structure with a diffraction angle at 2 thetas 11.93°, 13.97°, 20.87°, and 27.71°. Introducing ZrSe increased the peak intensity, signifying improved film crystallinity. Time significantly affected the electrical parameters and thickness of SrSe/ZrSe super-lattice. The film's absorbance decreases as its wavelength increases. The film's transmittance increases with wavelength. The SrSe/ZrSe synthesized at normal time had a bandgap energy of 2.50 eV. As the deposition time increased, the bandgap energy decreased to 2.39 - 2.22 eV.

G R A P H I C A L   A B S T R A C T
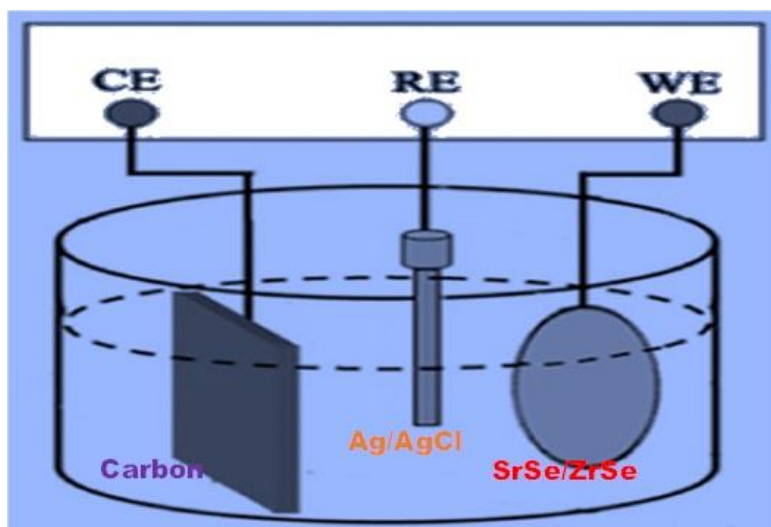
* Corresponding author: Ikhioya, Imosobomeh Lucky
✉ E-mail: imosobomeh.ikhioya@unn.edu.ng

Introduction

The distinct properties of II-VI materials made them applicable in optoelectronic devices. ZrSe has a band gap of 1.20 eV [1] and low optical absorption with a high refractive index. ZrSe can be doped with distinct elements to form a heterojunction. ZrSe has been studied for its electronic, catalytic, and thermoelectric properties. A stable $ZrSe_2$ monolayer comprises one plane of Zr atoms sandwiched between two slabs of Se atoms [2]. Monolayers stack weakly despite the strong bonding between Zr and Se atoms [3]. A wide range of technological applications rely on the unique properties of alkaline-earth chalcogenides [4]. SrSe thin films are being studied as a blue light source for electroluminescent devices. SrSe's optical properties have been hard to measure because of a lack of suitable single crystals [5]. The nonlinear optical coefficient of SrSe is high. The preferred material for optical devices is SrSe due to its remarkable thermal shock resistance [4]. SrSe could be used in photoelectric applications like LEDs and lasers. The use of the electrochemical deposition method is on the rise. This technique made it possible to cultivate thin films of SrSe/ZrSe super-lattice. By using the electrochemical deposition method, the entry of elements is regulated. The lattice constant of FTO is compatible with SrSe/ZrSe. Film characterization or device performance is improbable to be disrupted by the FTO substrate because of its transparency and conductivity.

Jiang *et al*. [4] utilized molecular beam epitaxy to grow a SrSe thin film on a BaF_2 ~111 and measured its optical properties. The SrSe thin film quality was evaluated by X-ray diffraction, which indicated a full width at half the maximum value of 310. The SrSe thin film had indirect band gaps, measured from 16 to 300 K. The spectra were determined by fitting the transverse optical phonon reflection bands. Zhao *et al.* [1] study used density functional theory to analyze doped $ZrSe_2$ monolayer. $ZrSe_2$ monolayers doped with nitrogen or phosphors are nonmagnetic metals. Mn-mono-doped $ZrSe_2$ monolayer is a magnetic semiconductor having a smaller direct band gap of 0.378 [6-12]. Metallic systems with intense magnetic moments are formed after codoping with Manganese, Nitrogen, and Manganese and Phosphor. Manganese dopant atoms create the polarized charges, while Selenium and nitrogen or phosphor atoms make minor contributions. It has been discovered that the dopant Manganese atoms and the neighbouring Selenium atoms are coupled antiferromagnetically [7]. Non-metal atoms are more easily incorporated in Zr-rich conditions in a monolayer of $ZrSe_2$. These results are significant because they pave the way for creating spintronic devices that rely on $ZrSe_2$.

A range of methods, including metal-organic chemical vapour deposition, have been employed in the synthesis of SrSe and ZrSe materials [1,8], Epitaxial growth [2,9], a molecular beam [4], and electrochemical deposition method [10], [12-15]. Electrochemical deposition is a standout process for production due to its improved photo-electrochemical and electrocatalytic capabilities. The approach is gaining interest because it's direct, inexpensive, environmentally safe, and non-polluting [16]. Electrochemical deposition involves loading the electrolyte solution into an electrochemical cell, where the electrode used is a substrate made of fluorine-doped tin oxide (FTO). Applying voltage results in the chemical polymerization of the electrolyte onto the FTO. Electrochemical deposition is inexpensive and enhances bonding between the coating material and substrate. An ionic liquid solution is used with FTO as a working electrode in an electrochemical cell to accomplish the electrodeposition of conductive substrates. Achieving uniform film thickness and cost reduction through electrochemical deposition parameter control [17-19]. Electrochemical deposition can be a promising technology for creating high-aspect ratio micro-tools of different

materials if the metal deposition is localized directly from small and shaped electrodes. Using this technology has made fabricating microelectrodes for micro-machining applications simpler and cheaper. This method enables easy fabrication of 3D microstructures on high-strength metals. Electrochemical deposition can cause metallic ions to transform into a solid metal and adhere to the cathode surface if the electrolyte solution receives sufficient electric current. Charged ions are formed within the electrolyte when a metallic salt is dissolved in water. An acidic metallic salt solution is used as electrolyte, with an anode submerged. The cathode, the deposited electrode, is placed above the anode. Applying a voltage pulse ensures successful localization of the deposition. The micro-tool's electro-chemically deposited structure porosity and accuracy can be controlled by adjusting process parameters such as voltage, pulse frequency, duty ratio, electrode gap, and mask. Various materials, such as metals, metal alloys, conductive polymers, and semiconductors, can be used to create micro-tools and micro-features through this process for various purposes [20].

This study employed the efficient electro-chemical deposition method to synthesize the SrSe/ZrSe material. We use various analytical techniques like X-ray diffraction, UV-visible spectroscopy and four-point probe to measure the photovoltaic potential of the material.

Experimental details

Materials

The materials used for the synthesis and characterization of strontium selenide/ zirconium selenide superlattice (SrSe/ZrSe) thin films are; strontium chloride ($SrCl_2.6H_2O$), Zirconium (IV) oxychloride octahydrate ($ZrOCl_2.8H_2O$), selenium (IV) oxide (SeO_2), Acetone, hydrochloric acid (HCl), distilled water, Power supply, Multimeter, Carbon electrode,

Fluorine doped tin oxide as substrate (FTO), Potentiostat which supplies a DC voltage in a two-electrode cell setup, electrolyte solution with (0.1 M, 20 mL) of strontium chloride ($SrCl_2.6H_2O$), (Sigma Aldrich, 99.9%), (0.1 M, 20 mL) of Zirconium (IV) oxychloride octahydrate ($ZrOCl_2.8H_2O$) (Sigma Aldrich, 99.9%), and (0.1 M, 10 mL) of selenium (IV) oxide (SeO_2) (Sigma Aldrich, 99.9%) was used to conducting the electrochemical deposition of strontium selenide/ zirconium selenide super-lattice (SrSe/ZrSe).

Preparation of FTO substrate

We deposited films of strontium selenide/ zirconium selenide superlattice (SrSe/ZrSe) on the FTO substrate, which had a sheet resistance of roughly 16.5 Ω/m. The area covered by the FTO-immersed region was approximately 2.5 cm². FTO glasses underwent 15-minute ultrasonic baths of ethanol, acetone, distilled water, and ammonia water. Afterward, the glasses were put in an electric thermostatic oven at 70 °C to dry.

Synthesis of strontium selenide/ zirconium selenide super-lattice (SrSe/ZrSe)

The electrochemical deposition setup had a DC supply to a three-electrode cell with a platinum CE, Ag/AgCl RE, and FTO WE (Figure 1). Deposition lasted for 5 seconds at a constant voltage of 10 V. The experiments were conducted at a constant room temperature. A potentiostat window was used to test strontium selenide/ zirconium selenide super-lattice (SrSe/ZrSe) films for 5 seconds at 29 °C and 4.8 pH with a -210 mV against a saturated calomel electrode. The solvents were placed in a 100 mL beaker while the deposition process was taking place at 10 V. To release the tension of the material, the resulting samples were heated to 350 °C for 30 min. In a 2theta range of 10° to 30°, the X-ray diffractometer was used to examine the crystal

structures and orientations of irradiated and unirradiated films.

Characterization of the films

The deposited films were characterized using suitable equipment and techniques to thoroughly study their optical, structural, and surface morphology. Using a 756S UV-visible spectrophotometer, the absorbance wavelength was measured in the optical spectral ranges from 300 nm to 110 nm. The surface morphology and chemical composition of the films were analyzed using the SEM technique. To study the electrical properties of deposited SrSe/ZrSe films, the Jandel four-point probe technique was utilized, measuring voltage changes across the inner probes as current flowed between the outer probes. The sheet resistivity and conductivity of the grown thin films at room temperature were calculated.
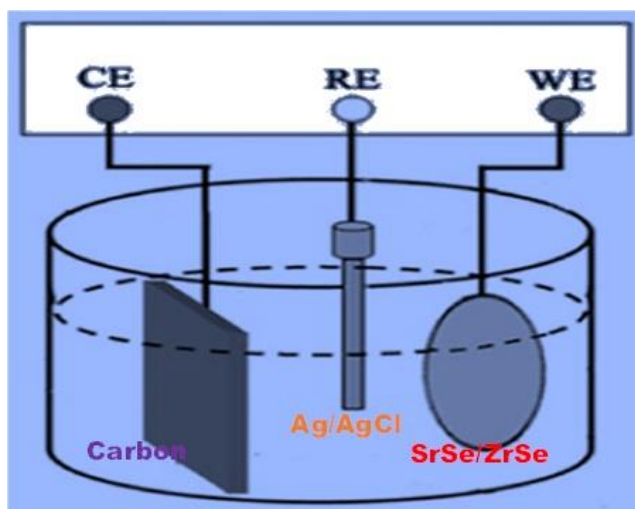

Figure 1. Schematic illustration of the electrochemical deposition technique

Result and Discussions

X-ray diffraction (XRD) result of SrSe/ZrSe

Figure 2 displays the XRD spectrum of SrSe/ZrSe superlattice materials deposited at different times. The spectrum indicates four crystal planes, namely (101), (102), (111), and (112). From the XRD pattern analysis, it can be observed that the sample has a polycrystalline cubic structure, with distinct diffraction peaks occurring at 2 thetas angles of 11.93^o, 13.97^o, 20.87^o, and 27.71^o. The crystallinity of films was found to have improved with the introduction of ZrSe, which was observed from the increased peak intensity in superlattice films. Ikhioya *et al.,* [21,22] also reported cubic structures after synthesizing CdSe/ZnSe superlattice films via the electrochemical deposition. Table 1 displays the diffraction planes, lattice spacing, lattice constant, FWHM, grain size, and dislocation density for various SrSe/ZrSe super-lattice material samples obtained from XRD. Table 1 illustrates that the lattice spacing decreases with increased deposition time, indicating that higher deposition time results in a more closely packed or denser SrSe/ZrSe material. The material's lattice constant decreases along with the reduction in grain size and dislocation density as the deposition time increases. The structural properties of the material were found to improve with an increase in deposition time. The lattice constant of the material synthesized at 100 s is lower. An increase in deposition time leads to a

rise in the slope of the Williamson Hall plot. The diffraction angle's peak becomes more prominent as the deposition time increases, leading to a decrease in dislocation density and an increase in grain size.
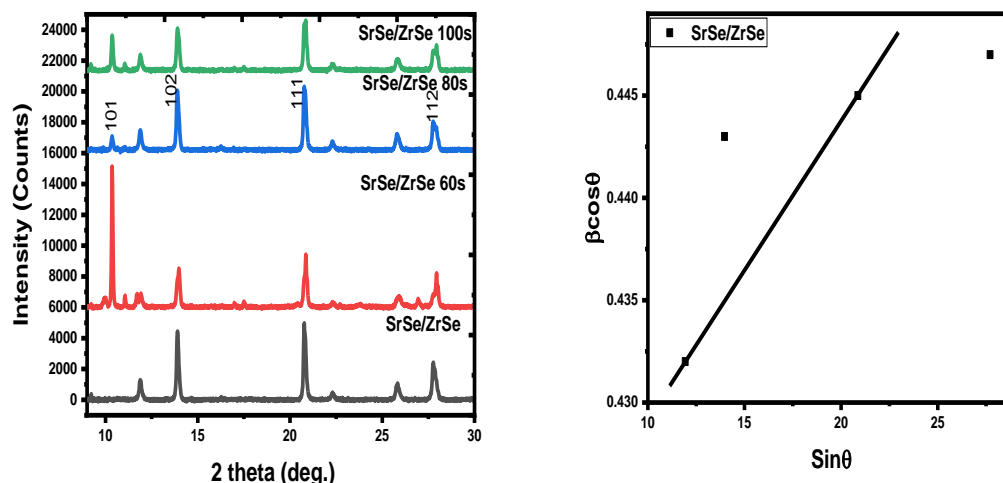

Figure 2. XRD spectrum of SrSe/ZrSe

Table 1. Structural parameters of SrSe/ZrSe

Films	2θ (degree)	(hkl)	d-spacing (Å)	Lattice constant (a)	FWHM (β)	Grain Size, D (nm)	Dislocation density, σ
SrSe/ZrSe	11.93	101	7.411	12.836	0.432	3.227	2.925
SrSe/ZrSe 60s	13.97	102	6.333	12.666	0.443	3.153	3.063
SrSe/ZrSe 80s	20.87	111	4.252	8.504	0.445	3.168	3.034
SrSe/ZrSe 100s	27.71	112	3.216	7.191	0.447	3.194	2.984

Electrical properties of SrSe/ZrSe deposited at a different time interval

The impact of the time intervals during which the SrSe/ZrSe super-lattice films were deposited on both their electrical parameters and thickness is evident in Table 2. It has been observed that with an increase in the deposition time from 60 to 100 s, the electrical resistivity of the films decreases. The thickness of the films has also decreased from 208.98 nm to 189.02 nm, increasing the electrical conductivity of the films. Figure 3 illustrates the correlation between the thickness of the film and the relationship between its resistivity and conductivity. Due to their high conductivity, the SrSe/ZrSe thin materials have been identified as great for use in solar cells and photovoltage applications.

Table 2. Electrical parameters of SrSe/ZrSe

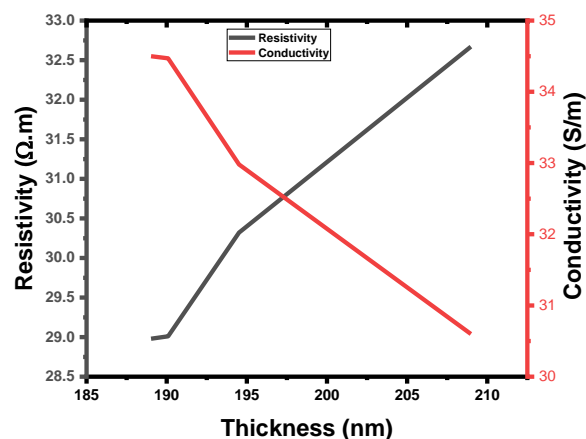| Films	Thickness, t(nm)	ρ (Ω.m) x 10^4	σ (S/m) x 10^3
SrSe/ZrSe	208.98	32.67	30.60
SrSe/ZrSe 60s	194.51	30.32	32.98
SrSe/ZrSe 80s	190.09	29.01	34.47
SrSe/ZrSe 100s	189.02	28.98	34.50

Figure 3. Resistivity and conductivity vs. thickness

Optical analysis of SrSe/ZrSe on time variations

The optical absorbance of a SrSe/ZrSe superlattice produced at different deposition times is illustrated in Figure 4 (A1). The absorbance of the films exhibits a sharp increase because there was an increase in the period of film deposition. The absorbance of the spectrum increases with a longer deposition time. As depicted in the plot, it is evident that the time of deposit plays a crucial role in the characteristics of synthesized films, and the examples further support this. As the duration of deposition increases, there is a corresponding increase in the absorbance of the films; conversely, reducing the duration of deposition results in a decrease in the absorbance of the films. Absorbance refers to the amount of light absorbed by a material or solution, typically measured by a spectro-photometer. The electronic industries benefit from a lower absorbance of films, making them ideal for solar panels and lighting systems. However, a greater absorbance of films is more suitable for photovoltaic applications. In Figure 4 (A2), you can see a graphical representation of the optical transmittance of a superlattice made of SrSe/ZrSe, created by deposition at different times. The sharp increase in the transmittance of the films is an increase in the time of film deposition. Through the discovery process, it has been found that the transmittance of the films decreases as the deposition time increases. The film synthesized at the regular time exhibits the highest transmittance in the spectrum. The plot depicts that the time of deposit plays a vital role in the synthesized films, which these examples further support this fact. The time of deposition directly affects the film's transmittance, as with an increase in deposition time, the transmittance decreases, and with a decrease in deposition time, the transmittance increases. In the electronic industries, the production of solar panels and lighting systems requires films with lower transmittance, whereas for photovoltaic applications, films with higher transmittance are considered ideal. The optical reflectance of a SrSe/ZrSe superlattice is shown in Figure 4 (A3), which was created at different deposition times. As the time for film deposition has increased, there has been a noticeable and sharp increase in the reflectance of the films. The research has discovered that as the deposition time increases, the reflectance of the films also increases, and the lowest reflectance is observed when the film is synthesized during the usual time. The plot provides evidence that the time of deposit has a notable influence on the synthesized films, and these observations further support this. An

increase in the deposition time leads to an increase in the reflectance of the films, while a decrease in the deposition time results in a decrease in the reflectance of the films. Since the lower reflectance of the films is more advantageous to produce solar panels and lighting systems in the electronic industries, on the other hand, the higher reflectance of the films is considered to be more appropriate for photovoltaic applications.
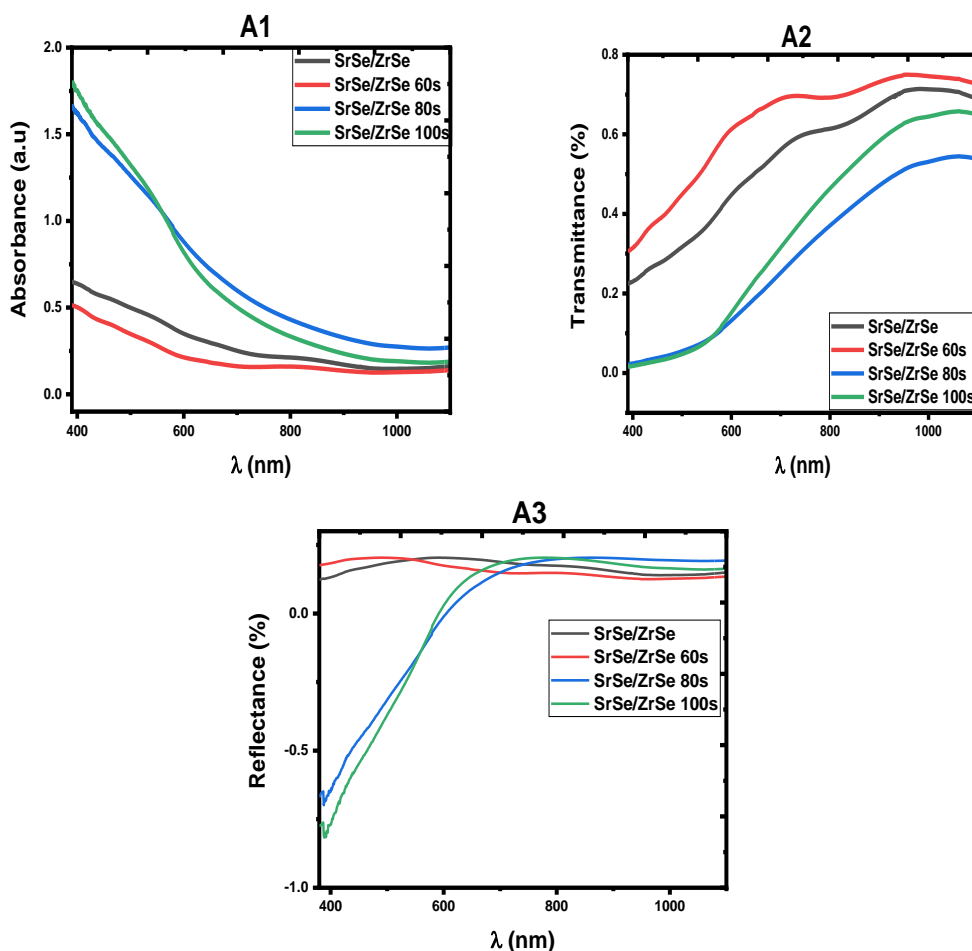
Figure 4. A1-absorbance, A2-transmittance, and A3-reflectance Vs wavelength

Figure 5 illustrates the absorption coefficient squared of the SrSe/ZrSe super-lattice films. The SrSe/ZrSe synthesized at the normal time was found to have a bandgap energy of 2.50 eV, whereas those synthesized at different times of deposition exhibited a bandgap energy of 2.39 - 2.22 eV, showing that the energy bandgap decreases as the time of deposition increases.

The refractive index of a SrSe/ZrSe superlattice, which was produced at different deposition times, is illustrated in Figure 6 (A4). As the period of film deposition increases, the refractive index of the films shows a sharp increase. - The spectra analysis revealed that the film synthesized within the normal time frame had the highest refractive index, whereas an increase in deposition time resulted in a decrease in refractive index. As evidenced by the plot, the time of deposit plays a significant role in influencing the quality of the synthesized films. As the time of deposition increases, the refractive index of the films decreases, whereas decreasing the time of deposition results in an increasing refractive index of the films. The films with higher refractive indices are not suitable for electronic industries' lighting systems and solar

panels, but these films are perfect for photovoltaic applications due to their greater refractive index. The graph shown in Figure 6 (A5) illustrates how the extinction coefficient of the SrSe/ZrSe superlattice varies at different deposition times. When the deposition time of the films was increased, the extinction coefficient of the films showed a sharp increase. Upon analysis of the films, it was discovered that the

extinction coefficient rose in correlation with the increase in deposition time. The film that was synthesized during the normal time, however, exhibited the lowest extinction coefficient in the entire spectrum. The impact of synthetic films is significantly influenced by the duration of deposition time as demonstrated by these findings.
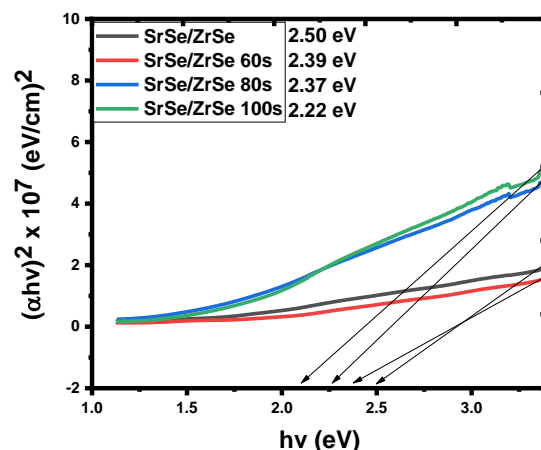
Figure 5. Band-gap energy
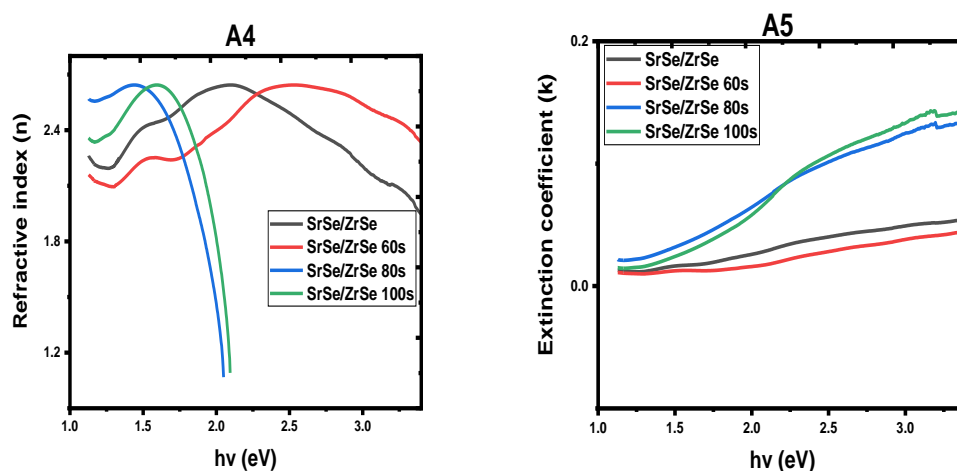
Figure 6. Plot of extinction coefficient Vs photon energy of SrSe/ZrSe at different time

Surface morphology of SrSe/ZrSe

Figure 7 shows the surface morphology of SrSe/ZrSe materials. The surface morphology analysis of the SrSe/ZrSe materials revealed nano clusters. The SrSe/ZrSe material transformed from nano clusters to nanoflakes. The materials were found to contain clusters of

nanoparticles that were larger, resulting in a rise in surface energy. The material clumped together because of defects caused by extended deposition time. The surface dislocation resulted in a disturbance in the lattice orientation [23-25]. The material's compact morphology makes it an excellent option for energy storage. Figure 8 illustrates the elemental composition of

SrSe/ZrSe. The elements comprise strontium, zirconium, and selenium. Silicon and calcium were observed because of the FTO substrate during synthesis.
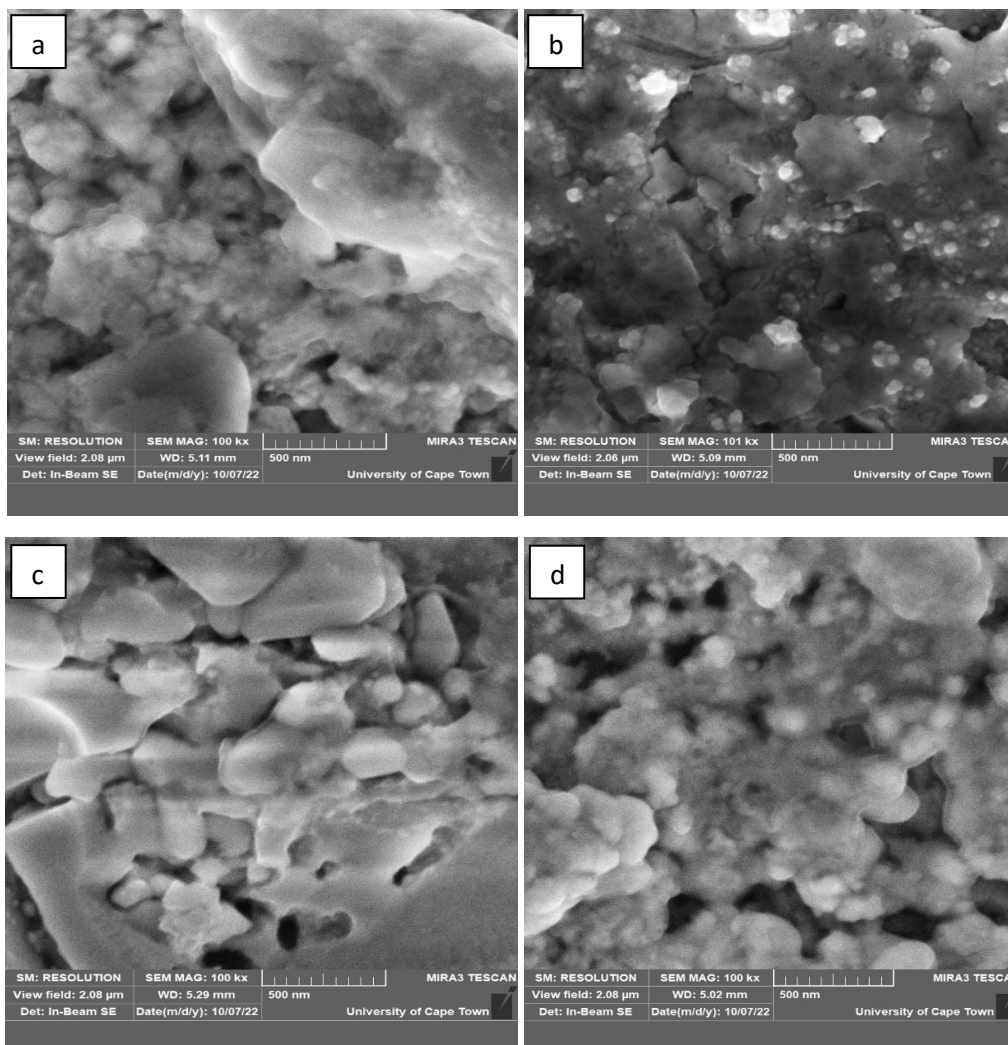

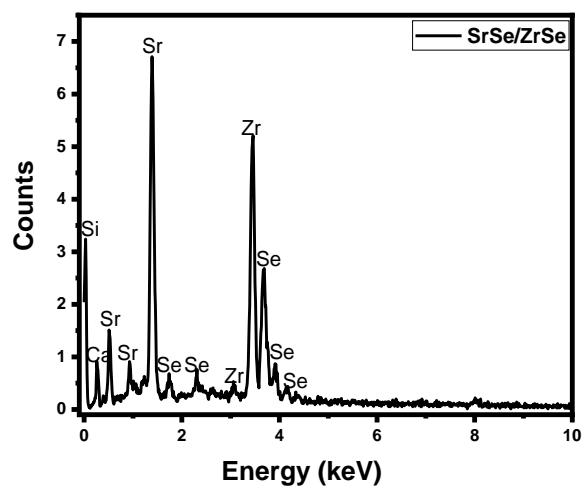**Figure 7.** SEM of SrSe/ZrSe-(a), SrSe/ZrSe 60s-(b), SrSe/ZrSe 80s-(c), and SrSe/ZrSe 100s-(d)

Figure 8. EDXs of SrSe/ZrSe

Conclusion

We have successfully synthesized SrSe/ZrSe super-lattice via an electrochemical deposition technique. The XRD spectrum reveals a polycrystalline cubic structure with a diffraction angle at 2 thetas 11.93°, 13.97°, 20.87°, and 27.71°. The introduction of ZrSe to form the super-lattice films was observed to improve the crystallinity of films as seen from the increased peak intensity. The film thickness and electrical properties of the SrSe/ZrSe super-lattice reveal that the voltage strongly influenced the electrical parameters and the thickness. The film's absorbance decreases as its wavelength increases. The transmittance of the film demonstrates that the films' transmittance increases as their wavelength increases. The transmittance of the pristine in the plot exhibits the maximum transmission as light radiation increases, and the transmittance spectra of the films change significantly when the deposition time varies. The SrSe/ZrSe synthesized at the normal time was found to have a bandgap energy of 2.50 eV, whereas those synthesized at different times of deposition exhibited a bandgap energy of 2.39 - 2.22 eV, showing that the energy bandgap decreases as the time of deposition increases

Acknowledgment

Disclosure statement

The authors declare that they have no conflict of interest.

Orcid

Imosobomeh Lucky Ikhioya iD: 0000-0002-5959-4427

References

[1] X. Zhao, H. Zhang, T. Chen, Y. Gao, H., Wang, T. Wang, S. Wei, *Superlattices Microstruct.,* **2018**, *120*, 659–669. [CrossRef], [Google Scholar], [Publisher]

[2] Y. Tian, M. Zheng, Y. Cheng, Z. Yin J., Jiang G., Wang, J. Chen, X. Li, J. Qi, X. Zhang, *J. Mater. Chem. C*, **2021**, *9*, 13954–13962, [CrossRef], [Google Scholar], [Publisher]

[3] A.S. Golub, Y.V. Zubavichus, Y.L. Slovokhotov, Y.N. Novikov, *Usp. Khim.*, **2003**, *72*, 138–158. [CrossRef], [Google Scholar], [Publisher]

[4] L.F. Jiang, W.Z. Shen, H.Z. Wu, *J. Appl. Phys.*, **2002**, *91*, 9015–9018. [CrossRef], [Google Scholar], [Publisher]

[5] P. A. Lee, G. Said, R. Davis, T.H. Lim, *J. Phys. Chem. Solids*, **1969**, *30*, 2719–2729. [CrossRef], [Google Scholar], [Publisher]

[6] G. Ding, G. Y. Gao, Z. Huang, W. Zhang, K. Yao, *Nanotechnology*, **2016**, *27*, 375703. [CrossRef], [Google Scholar], [Publisher]

[7] X. Zhou, K.H.L. Zhang, J. Xiong, J.H. Park, J.H. Dickerson, W. He, *Nanotechnology*, **2016**, *27*, 192001. [CrossRef], [Google Scholar], [Publisher]

[8] Z. Muhammad, M.W. Ali, I.A. Mir, Q.U. Khan, L. Zhu, *Nanotechnology*, **2020**, *31*, 235704. [CrossRef], [Google Scholar], [Publisher]

[9] R. Yue, A.T. Barton, H. Zhu, A. Azcatl, L.F. Pena, J. Wang, X. Peng, N. Lu, L. Cheng, R. Addou, S. McDonnell, *ACS Nano*, **2015**, *9*, 474–480. [CrossRef], [Google Scholar], [Publisher]

[10] S. O. Samuel, M.L.E. Frank, E.P. Ogherohwo, A. Ekpekpo, J.T. Zhimwang, I.L. Ikhioya, *East Eur. J. Phys.*, **2023**, *2023*, 189–196. [CrossRef], [Google Scholar], [Publisher]

[11] S.O. Samuel, C.K. Ojoba, E.P. Ogherohwo, E.O. Ojegu, J.T. Zhimwang, A. Ekpekpo, I.L. Ikhioya, *J. Indian Chem. Soc.*, **2023**, *100*, 100992. [CrossRef], [Google Scholar], [Publisher]

[12] S.O. Samuel, F.E. James, I.L. Ikhioya, *Mater. Res. Innov.*, **2023**, 1–11. [CrossRef], [Google Scholar], [Publisher]

[13] I. Rufus, A. Peter, S.O. Aisida, I.L. Ikhioya, *Results Opt.*, **2023**, *12*, 100464. [CrossRef], [Google Scholar], [Publisher]

[14] A. Heidaripour, F. Salmani, *Asian J. Green Chem.*, **2024**, *8*, 15–24. [CrossRef], [Publisher]

[15] M. Ahmadlouydarab, S. Javadi, F.A.A. Darab, *Adv. J. Chem. A*, **2023**, *6*, 352–365. [CrossRef], [Publisher]

[16] P. Prabukanthan, M. Sreedhar, S. Thamaraiselvi, G. Harichandran, P. Seenuvasakumaran, M.M. Hanafiah, C. Fernandez, *J. Mater. Sci. Mater. Electron.*, **2021**, *32*, 6331–6343. [CrossRef], [Google Scholar], [Publisher]

[17] J. Joo, J. K. Lee, J. S. Baeck, K. H. Kim, E. J. Oh, J. Epstein, *Synth. Met.*, **2001**, *117*, 45–51. [CrossRef], [Google Scholar], [Publisher]

[18] S.S. Kundale, G.U. Kamble, P.P. Patil, S.L. Patil, K.A. Rokade, A.C. Khot, K.A. Nirmal, R.K. Kamat, K.H. Kim, H.M. An, T.D. Dongale, *Nanomaterials*, **2023**, *13*, 1879. [CrossRef], [Google Scholar], [Publisher]

[19] S.M. Mousavi, J.B. Raoof, M. Ghani, *J. Iran. Chem. Soc.*, **2023**, *20*, 2285–2295, , [CrossRef], [Google Scholar], [Publisher]

[20] B. Bhattacharyya, *Chapter 2–electrochemical machining: macro to micro*, William Andrew Publishing, **2015**, pp. 25–52. [CrossRef], [Google Scholar], [Publisher]

[21] I.L. Ikhioya, A.J. Ekpunobi, *J. Niger. Assoc. Math. Phys.*, **2014**, *28*, 289–296. [Google Scholar]

[22] R.O. Ijeh, A.C. Nwanya, A.C. Nkele, I.G. Madiba, A.K.H. Bashir, A.B.C. Ekwealor, R.U. Osuji, M. Maaza, F. Ezema, *Ceram. Int.*, **2020**, *46*, 10820–10828, [CrossRef], [Google Scholar], [Publisher]

[23] A.P.V. Rakkini, K. Mohanraj, *Inorg. Nano-Metal Chem.*, **2022**, *52*, 570–575. [CrossRef], [Google Scholar], [Publisher]

[24] A.M. Sargar, N.S. Patil, S.R. Mane, S.N. Gawale, P.N. Bhosale, *Int. J. Electrochem. Sci.*, **2009**, *4*, 887–894, [CrossRef], [Google Scholar], [Publisher]

[25] M. Wang, Y. Zheng, L. Guo, X. Chen, H. Zhang, D. Li, *Nanomaterials*, **2019**, *9*, 1419. [CrossRef], [Google Scholar], [Publisher]